HHS Public Access

Author manuscript

J Bone Miner Res. Author manuscript; available in PMC 2020 March 31.

Published in final edited form as:

J Bone Miner Res. 2019 May ; 34(5): 939–954. doi:10.1002/jbmr.3667.

Lack of myosin X enhances osteoclastogenesis and increases cell surface Unc5b in osteoclast-lineage cells

Bo Wang[1,2,3,4], **Jin-Xiu Pan**[1,2,3], **Huali Yu**[1,3,5], **Lei Xiong**[1,2,3], **Kai Zhao**[1,3], **Shan Xiong**[3], **Jun-Peng Guo**[3], **Sen Lin**[3], **Dong Sun**[1,2], **Lu Zhao**[1,3,5], **Haohan Guo**[1,2,3], **Lin Mei**[1,2,3], **Wen-Cheng Xiong**[1,2,3,#]

[1]Department of Neurosciences, School of Medicine, Case Western Reserve University, Cleveland, OH 44106, USA

[2]Louis Stokes Cleveland Veterans Affairs Medical Center, Cleveland, OH 44106, USA

[3]Department of Neuroscience and Regenerative Medicine, Medical College of Georgia, Augusta University, Augusta, GA 30912, USA

[4]Department of Orthopaedic Surgery, Tongji Hospital, Tongji Medical College, Huazhong University of Science and Technology, Wuhan, Hubei, China

[5]Key laboratory of Molecular Epigenetics of Ministry of Education, Institute of Cytology and Genetics, Northeast Normal University, Changchun, Jilin, China

Abstract

Normal bone mass is maintained by balanced bone formation and resorption. Myosin X (Myo10), an unconventional MyTH4-FERM domain containing myosin, is implicated in regulating osteoclast (OC) adhesion, podosome positioning, and differentiation in vitro. However, it lacks of evidence for Myo10's in vivo function. Here we show that mice with Myo10 loss of function, $Myo10^{m/m}$, exhibit osteoporotic deficits, which are likely due to the increased OC genesis and bone resorption, as bone formation is unchanged. Similar deficits are detected in OC-selective Myo10 conditional knockout (cKO) mice, indicating a cell autonomous function of Myo10. Further mechanistic studies suggest that Unc5b protein levels, in particularly its cell surface level, are higher in the mutant OCs, but lower in RAW264.7 cells or HEK293 cells expressing Myo10. Suppressing Unc5b expression in BMMs from $Myo10^{m/m}$ mice by infection with lentivirus of Unc5b shRNA markedly impaired RANKL induced OC genesis. Netrin-1, a ligand of Unc5b, increased RANKL induced OC formation in BMMs from both wild type and $Myo10^{m/m}$ mice.

[#]Correspondence author: Wen-Cheng Xiong, PhD, Department of Neurosciences, School of Medicine, Case Western Reserve University, Cleveland, OH 44106, USA. Wen-Cheng.Xiong@case.edu Phone: 216-368-4865.

Authors' roles: Study Design: WCX, LM, and BW. Study Conduct: BW. Data Collection: BW, JP, HY, LX, KZ, SX, JG and SL. Data analysis: BW, LZ, LX and HG. Data interpretation: BW, KZ, DS and WCX. Drafting manuscript: BW and WCX. Revising manuscript: BW, JP, KZ, LX and WCX. Approving final version of manuscript: BW, JP, HY, LX, KZ, SX, JG, SL, DS, LZ, HG, LM and WCX. WCX takes responsibility for the integrity of the data analysis.

Disclosures

All authors of this manuscript state that they have no conflict of interest

Taken together, these results suggest that Myo10 plays a negative role in OC formation likely by inhibiting Unc5b cell surface targeting, and suppressing Netrin-1 promoted OC-genesis.

Keywords

Myosin X; bone remodeling; osteoclast; Unc5b; cell surface

Introduction

Bone remodeling involves dynamic balance between bone formation by osteoblasts (OB) and bone resorption by osteoclasts (OC),[1] which is important for maintenance of normal bone mass. Osteoclasts are differentiated from hematopoietic bone marrow macrophages (BMMs) and activated to resorb bone by different factors, among which Receptor activator of NF-κB ligand (RANKL) is one of the best studied.[2]

Myosin X (Myo10) is an unconventional MyTH4-FERM domain containing myosin that is widely expressed in various tissues.[3] It acts as an actin-based molecular motor in filopodia formation, cell migration, cell polarization, mitosis, cancer invasion and metastasis.[4-8] The MyTH4-FERM domain mainly functions in binding to Myo10 cargo proteins such as deleted in colorectal cancer (DCC), neogenin, integrins, N-cadherin, and BMP6 receptor (ALK6).[3, 9-11] In addition, this domain also interacts with microtubules.[12] What's more, Myo10 is found to play a role in OC attachment and podosome positioning by direct linkage of actin to the microtubule network.[13] Myo10 is also report to regulate the formation of tunneling nanotubes.[14] But the impacts of Myo10 on bone remodeling in vivo remains largely unknown.

Via regulating the distribution of DCC, a receptor for netrin-1, Myo10 is implicated in netrin-1-DCC signaling and function in developing brain.[3] Netrin-1 is a secreted protein functions in axon guidance, cell migration, morphogenesis and angiogenesis during development.[15-17] It can trigger attraction by binding to DCC or repulsion through binding to Unc5 family receptors.[18, 19] Unc5 family contains Unc5a, Unc5b, Unc5c and Unc5d receptors, and among which, Unc5b is the most abundant in OCs. In addition to mediating axon repulsion of neuronal growth cones, functions of Unc5b include negatively regulating vascular branching during angiogenesis, apoptosis induction, and retraction of tip cell filopodia on endothelial growth cones. [18, 20-23] Recent studies implicate Unc5b in osteoclastogenesis. Aránzazu Mediero et. al[24] have showed that weekly injection of anti-Netrin-1 or anti-Unc5b antibodies significantly reduce the inflammatory infiltration and the number of TRAP-positive OCs, thus attenuating the particle-induced osteolysis. In addition, the blockade of netrin-1 or Unc5b by monoclonal antibodies also decreases the number of OCs, preventing bone destruction and reducing the severity of K/BxN serum transfer-induced arthritis.[25] The anti-OCs and bone protective effects by anti-Netrin-1 or anti-Unc5b antibodies are also observable in a murine model of multiple myeloma.[26] Moreover, netrin-1 and Unc5b expression are increased during OC differentiation, and blockade of netrin-1 or Unc5b prevents OC differentiation from both murine and human precursors.[27]

While these observations suggest a positive role of netrin-1-Unc5b pathway in OC genesis, the exact function of Myo10 in this pathway remains to be explored.

Here we provide evidence for Myo10 to regulate bone remodeling. Myo10 is expressed in both OB and OC lineage cells. By micro-CT (μCT) and bone histomorphometric analyses of a Myo10 loss of function mutant mouse line (named as $Myo10^{m/m}$)(also called $Myo10^{tm1a/tmla}$ in previous report[28]), we observed osteoporotic deficits in $Myo10^{m/m}$ mice. The osteoporotic deficits appear to be due in large to the increased OC differentiation and bone resorption, as no significant changes was detected in bone formation. The osteoporotic phenotypes are also detected in OC-selective Myo10 knockout mice, which are generated by breeding floxed Myo10 ($Myo10^{f/f}$) with LysM-promotor driven Cre mice ($Myo10^{LysM}$-cko mice hereafter). These results suggest a cell autonomous Myo10's function in suppressing OC differentiation. Further mechanistic studies indicate that Unc5b protein levels are increased in OCs from $Myo10^{m/m}$ mice. $Myo10^{m/m}$ BMMs exhibit more cell surface distribution of Unc5b, while expressing exogenous Myo10 reduces cell surface level of Unc5b. The increased OC formation in $Myo10^{m/m}$ BMMs is abolished by suppression of Unc5b expression. Taken together, these results suggest that Myo10 plays a negative role in OC formation, which is likely due to its attenuation of Unc5b targeting to the cell surface and thus inhibiting netrin-1-Unc5b signaling and function during OC genesis.

Materials and Methods

Reagents and animals

For immunoblotting analysis, the following primary antibodies were used: rabbit polyclonal anti-Myo10 (1:500) was generated as previously described,[3] rabbit monoclonal anti-Unc5b (#13851, 1:1000) from Cell Signaling Technology, rabbit polyclonal anti-Integrin β3 (#4702, 1:1000) from Cell Signaling Technology, rabbit polyclonal anti-Flag (F7425, 1:2000) from Sigma-Aldrich, rabbit polyclonal anti-FAK (sc-557, 1:500) from Santa Cruz Biotechnology, rabbit polyclonal anti-phospho-FAK (Tyr861) (44-626G, 1:1000) from ThermoFisher Scientific, rabbit polyclonal anti-Src (#2108, 1:1000) from Cell Signaling Technology, rabbit monoclonal anti-phospho-Src (Tyr416) (#04-857, 1:1000) from Millipore. Mouse monoclonal anti-RANK (sc-374369, 1:500) from Santa Cruz Biotechnology, mouse monoclonal anti-Integrin αV (#611012, 1:500) from BD Biosciences, mouse monoclonal anti-transferrin (sc-393595, 1:2000) from Santa Cruz Biotechnology, mouse monoclonal anti-GAPDH (ab9484, 1:5000) from Abcam, mouse monoclonal anti-β-actin (AC-15, 1:5000) from Novus Biologicals. For immunostaining analysis, the following primary antibodies were used: rabbit polyclonal anti-Flag (F7425, 1:1000) from Sigma-Aldrich, rabbit polyclonal anti-GFP (A-11122, 1:1000) from Invitrogen. Alexa Fluor 488- and 555-coupled secondary antibodies against rabbit and HRP-conjugated secondary antibodies against mouse or rabbit were purchased from Jackson ImmunoResearch Laboratories. Nuclei were stained with 4',6-diamidino-2-phenylindole (DAPI) (1:1000, Roche). Alexa Fluor 488 Phalloidin (A12379) was purchased from Thermo Fisher Scientific. Recombinant mouse netrin-1 (1109-N1) was purchased from R&D Systems.

$Myo10^{m/m}$ (also called $Myo10^{tm1a/tm1a}$) mice were generated by injection of mutant embryonic stem cells from Knockout Mouse Project (KOMP) that have an insertion of KO

cassette located in the intron between exon 26 and 27 of the Myo10 gene. Myo10 expression is markedly suppressed due to this insertion (Fig. 1, E and F). $Myo10^{m/m}$ mice appeared to express a truncated form of Myo10, containing the N-terminal head domain, but not the C-terminal regions (e.g., MyTH4 and FERM domains), according to RT-PCR analyses (data not shown). The $Myo10^{m/m}$ gene was identified by PCR genotyping using four primers below:

5′-GAAAAGGCGCATAACGATACCACG-3′,

5′-CCAACTGACCTTGGGCAAGAACAT-3′,

5′-CAGTGTAGGGTAGCGTTCCTCAG-3′,

5′-AGAGAACCGCCCATATTACACC-3′).

$Myo10^{m/m}$ mice were crossed with C57BL/6J mice for more than F6 generations. The floxed Myo10 ($Myo10^{f/f}$) mice were generated by crossing $Myo10^{m/m}$ with FLP mice. $Myo10^{f/f}$ mice were then crossed with LysM-Cre mice (purchased from The Jackson Laboratory, #004781) to generate $Myo10^{LysM}$-cko mice. All the experimental procedures were approved by the Institutional Animal Care and Use Committees at Case Western Reserve University (CWRU) and Augusta University in accordance with National Institutes of Health guidelines.

β-Gal staining

β-Gal staining was carried out as described previously.[29] In brief, frozen femur sections and cultured BMMs or BMSCs from P15 mice were fixed with 0.5% cold glutaraldehyde for 10 min on ice and incubated in X-gal staining solution (2 mM $MgCl_2$, 5 mM potassium ferricyanide, 5 mM potassium ferrocyanide and 0.1% X-gal) in the dark at 37°C for 12 hours. The slides were then rinsed, mounted in Permount (Thermo Fisher Scientific) and imaged using digital microscope (Axioplan 2; Carl Zeiss).

μCT

The microcomputed tomography (μCT) analysis was carried out as previously described.[30, 31] In brief, microarchitecture of the distal trabecular bone and midshaft cortical bone of the femur were measured by Scanco μCT 40 (Scanco Medical AG). Bones were placed vertically in 12-mm-diameter scanning holders and scanned at the following settings: 12 um resolution, 55 kVp energy, 145 μA intensity, and 200 ms integration time. For the cortical bone, the bone was scanned at the midshaft of the bone for a scan of 25 slices. The threshold for cortical bone was set at 329 and 3D reconstruction was performed using all the slices. Data were obtained on bone volume (BV), total volume (TV), BV/TV, total cross-sectional area (Tt.Ar), cortical bone area (Ct.Ar) and cortical bone area fraction (Ct.Ar/Tt.Ar). For the trabecular bone, the scan was started at the growth plate and consisted of 211 slices. 100 slices were outlined on the inside of the cortical bone, enclosing only the trabecular bone and marrow. The threshold for trabecular bone was set at 245 and the 3D analysis performed on the 100 slices. Data were obtained on BV/TV, trabecular number (Tb.N), trabecular separation (Tb.Sp) and trabecular thickness (Tb.Th).

Bone histomorphometric analysis

Bone histomorphometric analysis were performed as previously described.[32, 33] In brief, mouse tibias and femurs were fixed overnight in 10% buffered formalin, decalcified in 14% EDTA for two weeks, embedded in paraffin, sectioned and subjected to hematoxylin and eosin (H&E), safranin O and TRAP staining analysis. Bone histomorphometric perimeters were determined by measuring the areas situated at least 0.5 mm from the growth plate, excluding the primary spongiosa and trabeculae connected to the cortical bone.

In vivo dynamic bone histomorphometric analysis of bone formation

In vivo dynamic bone histomorphometric analysis were carried out by intraperitoneal injection of 10 mg/kg fluorochrome-labeled calcein green (Sigma-Aldrich) and then 50 mg/kg alizarin red (Sigma-Aldrich) (12 d interval) in 2-week-old mice. The mice were euthanized 2 days after the second injection and femurs were fixed in 70% ethanol overnight, embedded in methyl methacrylate, and sectioned at 7-10 μm. Images were obtained by using a 25x objective fluorescence microscope (LSM510, Carl Zeiss). The mineral apposition rate (MAR) and bone formation rate (BFR) were calculated from fluorochrome double-labels at the endocortical surfaces.

Measurements of serum levels of osteocalcin and deoxypyridinoline (PYD)

Mouse serum samples were collected and stored at −80°C until use. Mouse osteocalcin ELISA kit (Biomedical Technologies, Inc.) and Metra Serum PYD RIA kit (Quidel Corporation) were used to measure the serum osteocalcin and PYD respectively. All the assays were carried out according to the manufacturer's instructions. All the samples were measured in duplicate, and values were subjected to statistical analysis.

In vitro BMSCs and OB cultures

Whole bone marrow cells were flushed from long bones of 2-month-old $Myo10^{+/+}$ and $Myo10^{m/m}$ mice and plated on 100-mm tissue culture plates in DMEM containing 10% FBS and 1% penicillin/streptomycin (P/S). BMSCs were passed by trypsin digestion after 7 days and plated in densities of 1 x 10^4 /cm^2 for osteogenesis differentiation in osteogenic medium (DMEM containing 10% FBS, 1% P/S, 10 mM β-glycerophosphate, and 50 μM L-ascorbic acid-2-phosphate). Alkaline phosphatase (ALP) staining and quantification were performed 7 and 14 days after incubation.

In vitro BMMs and OC cultures

Whole bone marrow cells were flushed from long bones of 2-month-old $Myo10^{+/+}$ and $Myo10^{m/m}$ mice, plated on 100-mm tissue culture plates in α-MEM containing 10% FBS, 1% P/S and 10 ng/ml recombinant macrophage colony-stimulating factor (M-CSF), and incubated at 37°C with 5% CO_2 overnight. Nonadherent cells were collected and subjected to Ficoll-Hypaque gradient centrifugation for purification of BMMs. BMMs were passed and plated in densities of 5 x 10^4 /cm^2 for osteoclastic differentiation in OC differentiation medium (α-MEM containing 10% FBS, 1% P/S, 10 ng/ml M-CSF and 100 ng/ml recombinant RANKL). Mature OC (multi-nucleated, large-spread cells) began to form at day 4-5 after RANKL treatment. TRAP staining and quantification were then performed.

Western blot analysis

Immunoblotting analysis was performed as described previously. Cells were washed twice with ice-cold 1 X PBS and lysed with lysis buffer [50 mM Tris-HCl (pH 7.5), 150 mM NaCl, 1% Triton X-100, 0.1% SDS, 0.5% deoxycholate, and 1 mM EDTA, supplemented with protease inhibitors (1 ug/ml leupeptin and pepstatin, 2 ug/ml aprotinin and 1 mM PMSF) and phosphatase inhibitors (10 mM NaF and 1 mM Na_3VO_4)]. The lysates were centrifuged at 14,000g for 15 min at 4°C and protein concentration was determined with BCA protein assay kit (Thermo Fisher Scientific). Protein were resolved by 10% SDS-PAGE gel and transferred to PVDF membranes. The membranes were blocked and immunoblotted with indicated antibodies.

RNA isolation and Real-Time PCR analysis

Total RNA was isolated from target cells by TRIZOL extraction (Invitrogen). Quantitative PCR was performed with Quantitect SYBR Green PCR Kit (Bio-Rad) and analyzed with software (Option Monitor 3), according to manufacturer's instruction. For a complete list of primers used in this study, please refer to Table 1.

Immunofluorescence staining and confocal imaging

Cells were plated on coverslips, fixed with 4% paraformaldehyde (PFA) in PBS at room temperature for 15 min, permeabilized and blocked with 0.2% Triton X-100, 10% donkey serum in PBS at room temperature for 1 h, incubated with primary antibodies overnight at 4°C. The cells were then washed 3 times with 0.2% Triton X-100 in PBS and incubated in Alexa Fluor secondary antibodies at room temperature for 1 h. Finally, the samples were mounted with VECTASHIELD (vector laboratories) mounting medium and the confocal images were taken by Zeiss LSM 800 confocal microscope. In some cases, to label the plasma membrane, PFA fixed cells were immersed in Dil (D282, Thermo Fisher) working solution (120 μg/ml Dil in PBS with 4% glucose) at 37°C for 5 min and then, 4°C for 15min, which was then resolved to permeabilization and antibody incubation. For statistical analysis, the relative fluorescent intensity of Flag-Unc5b on the plasma membrane (colocalized with Dil) versus total or cytoplasm were quantified using ImageJ software. At least 20 cells were measured for each group.

Cell surface biotinylation

Cell surface biotinylation analysis was performed as described previously.[34] Cells were washed with ice cold PBS (+Ca/Mg) three times, and freshly prepared PBS (+Ca/Mg) containing 0.25 mg/ml EZ-Link™ Sulfo-NHS-SS-Biotin (Thermo Fisher Scientific) was added. After incubation at 4°C for 45 min with gentle shake, the reaction was terminated by addition of 10 mM Glycine. 20 min later the cells were washed three times with ice cold PBS (+Ca/Mg), lyzed with 500 ul of lysis buffer (50 mM Tris-HCl pH 7.5, 150 mM NaCl, 1% Triton X-100, 1% NP-40 supplemented with protease inhibitors), and incubated at 4°C for 1h on shaker. After centrifugation at 14000 rpm for 10 min at 4°C, the supernatants were transferred to pre-chilled tubes. Immunoprecipitation was started by adding 50 ul Streptavidin-Agarose beads (Pierce), rotating overhead at 4°C overnight. The beads were washed three times with ice cold lysis buffer, and the biotinylated proteins were eluted with

50 ul 1x loading buffer by boiling for 5 min. Eluates and non-biotinylated lysates were subjected to immunoblotting.

Plasmids and transient transfection

The pTT3 Unc5B-FLAG plasmid (#72195) was purchased from Addgene. The plasmids encoding GFP-tagged Full-length Myo10 (FL) and Headless Myo10 (HL, an isoform which lacks the motor domain) were generated as previously described.[3, 9] Flag-Netrin-1 plasmid was generated by insertion of chicken Netrin-1 into the pFlag-CMV1 vector. HEK293T and RAW264.7 cells were maintained in DMEM supplemented with 10% FBS and 1% P/S. Transfections were carried out using Lipofectamine 2000 (Invitrogen) according to manufactures instructions. 48 hours following transfection, cells were subjected to further analysis.

Netrin-1 conditioned medium preparation

Flag-Netrin-1 plasmid was transfected into HEK293T cells using Lipofectamine 2000 (Invitrogen) according to manufactures instructions. Eight hours following transfection, culture medium was changed into α-MEM without serum. 24 h later, the conditioned medium (CM) was collected, filtered and stored at −20°C.

Lentivirus packaging and infection of target cells

The control and Unc5b shRNA were inserted into the pLL3.7 lentiviral vector, which can express GFP for identification. For lentivirus packaging, control or Unc5b shRNA along with the psPAX2 (Addgene) and pMD2.G (Addgene) packaging plasmids were co-transfected into HEK293T cells. 48 h and 72 h later, viral supernatants were collected, filtered by 0.45 um filters (Millipore) and concentrated using Amicon Ultra-15 Centrifugal Filter Device (Millipore 100K MWCO). Primary cultured BMMs were infected with the concentrated virus for 24 h. And 72 h later after confirmation of infection efficacy, BMMs were treated with osteoclastogenic medium for osteoclastic differentiation.

Statistical analysis

All data were expressed as mean ± SD. The significance level was set at $P < 0.05$. Student's *t* test was used for statistical analysis.

Results

Osteoporotic deficits in Myo10$^{m/m}$ mice

To investigate functions of Myo10 in bone remodeling, we generated Myo10$^{m/m}$ mice which contained LacZ knocking-in in the intron of Myo10 gene between exon 26 and 27, so that LacZ expression is likely controlled by the Myo10 promoter (Fig. 1, A). The LacZ activity was detected in both trabecular and cortical bones of Myo10$^{m/m}$ mice (P15) but not in wild type control (Myo10$^{+/+}$) littermates (Fig. 1, B). Bone marrow stromal cells (BMSCs, precursors of OBs) and bone marrow macrophages (BMMs, precursors of OCs) from Myo10$^{m/m}$ mice but not Myo10$^{+/+}$ mice also showed positive LacZ activity (Fig. 1, C and D), implicating Myo10's expression in both OB and OC lineage cells. To confirm this view

and to verify the successful generation of Myo10$^{m/m}$ mice, Myo10 mRNA levels were detected by RT-PCR analysis using primers targeting the 3' terminus of Myo10 gene (Fig. 1, F), and Myo10 protein levels were examined by Western blot analysis (Fig. 1, E). The results showed successful deletion of the Myo10 gene expression in OB and OC lineage cells at both mRNA and protein levels (Fig. 1, E and F). Note that the relative mRNA copy numbers were higher in BMMs and OC than those in BMSCs and OB, complying with the relative protein levels of Myo10.

We next tested the influence of Myo10 on bone mass. μCT analysis was carried out to examine the femur bone mass and structures. Decreased trabecular bone volumes over total volumes (BV/TV), trabecular bone numbers (Tb.N) and trabecular thickness (Tb.Th), as well as increased trabecular separation (Tb.Sp) were observed in Myo10$^{m/m}$ mice, compared to that of Myo10$^{m/m}$ littermates (Fig. 2, A-E). While cortical BV/TV, total cross-sectional area (Tt.Ar), cortical bone area (Ct.Ar) and cortical bone area fraction (Ct.Ar/Tt.Ar) had no significant changes (Fig. 2, F-I). Further observations by H&E staining analysis of femur sections provided additional support for the decreased trabecular BV/TV in adult (2-month-old) Myo10$^{m/m}$ mice (Fig. 2, J and K). In addition, safranin O staining analysis exhibited similar morphology of growth plate between Myo10$^{+/+}$ and Myo10$^{m/m}$ mice (Supplement Fig. 1), suggesting little or no effect of Myo10 on chondrocyte differentiation and function. Taken together, Myo10 is an important regulator of bone mass.

No change of bone formation in Myo10$^{m/m}$ mice

As bone mass is determined by bone formation and bone resorption, we next examined both processes in Myo10$^{+/+}$ and Myo10$^{m/m}$ mice. For bone formation analysis, neonatal (2-week-old) littermates of Myo10$^{+/+}$ and Myo10$^{m/m}$ mice received two injections of calcein green and alizarin red fluorochrome labels, separated by a 12-d interval. Both endocortical (Ec.) (Fig. 3, A) and trabecular (Tb.) (Fig. 3, B) mineral apposition rate (MAR), mineral surface / bone surface (MS/BS), and bone formation rate (BFR) were analyzed in nondecalcified femur sections of the injected mice. No significant difference was observed in Ec.MAR, Tb.MAR, Ec.MS/BS, Tb.MS/BS, Ec.BFR and Tb.BFR between Myo10$^{+/+}$ and Myo10$^{m/m}$ mice (Fig. 3, A-H). The unchanged bone formation was further confirmed by comparable levels of serum osteocalcin (Fig. 3, I), a bone formation marker, in the mutant mice to that of controls. In vitro osteoblastogenesis assays of BMSCs derived from 2-month-old Myo10$^{+/+}$ and Myo10$^{m/m}$ mice also showed no significant difference of OB-differentiation detected by alkaline phosphatase (ALP) staining (Fig. 3, J-M). Taken together, these results suggest little or no effects of Myo10 on bone formation.

Increased bone resorption and OC formation in Myo10$^{m/m}$ mice

We next checked bone resorption in Myo10$^{+/+}$ and Myo10$^{m/m}$ mice. Serum levels of deoxypyridinoline (PYD), a bone resorption marker, was higher in Myo10$^{m/m}$ mice than that of littermate controls (Fig. 4, A), suggesting an increase of bone resorption. In line with this view is TRAP staining analysis of femur sections from adult (2-month-old) Myo10$^{+/+}$ and Myo10$^{m/m}$ mice, which also showed a significant increase in the number of TRAP^{+} OC per unit of bone surface (Fig. 4, B and C). We then checked whether Myo10 regulates OC formation in vitro. BMMs from Myo10$^{+/+}$ and Myo10$^{m/m}$ mice were treated with

macrophage colony-stimulating factor (M-CSF) and RANKL for 5 days to induce OCs. $Myo10^{m/m}$ cultures showed more and larger $TRAP^{+}$ OC (Fig. 4, D and E), and phalloidin immunofluorescence staining of actin ring structures also showed larger OCs with more nuclei numbers (Fig. 4, F and G). In further supporting an increased osteoclastogenesis in $Myo10^{m/m}$ mice was the observation of the increased mRNA levels of TRAP, Cathepsin K, MMP9 and Nfatc1 (Fig. 4, H-K), markers of OC. Together, these results suggest a crucial function of Myo10 in negatively regulating OC formation.

Similar osteoporotic deficit with elevated bone resorption and OC formation in OC-selective Myo10 knockout mice

To determine whether Myo10 regulates OC formation in a cell-autonomous manner, we generated $Myo10^{LysM}$-cko mice by crossing floxed Myo10 ($Myo10^{f/f}$) with lysozyme (LysM)-Cre mice which selectively express Cre in mature macrophages (precursors of OC) (Fig. 5, A).[35] Western blot analysis confirmed the diminished protein levels of Myo10 in BMMs and OCs but not BMSCs or OBs in $Myo10^{LysM}$-cko mice (Fig. 5, B). We next carried out μCT analysis to examine the femur bone mass and structures. Similar to the phenotypes detected in $Myo10^{m/m}$ mice, decreased trabecular bone volumes over total volumes (BV/TV), trabecular bone numbers (Tb.N) and trabecular thickness (Tb.Th), as well as increased trabecular separation (Tb.Sp) were observed in $Myo10^{LysM}$-cko mice, as compared with that of $Myo10^{f/f}$ littermates (Fig. 5, C-G). The cortical BV/TV, total cross-sectional area (Tt.Ar), cortical bone area (Ct.Ar) and cortical bone area fraction (Ct.Ar/Tt.Ar) had no significant changes (Fig. 5, H-K). Further, $Myo10^{LysM}$-cko mice showed increased serum levels of PYD (Fig. 5, N) and number of $TRAP^{+}$ OC per unit bone surface by TRAP staining of their femur sections (Fig. 5, L and M), demonstrating increased OC formation and bone resorption. Concomitantly, in vitro osteoclastogenesis assay also showed more and larger $TRAP^{+}$ OC in $Myo10^{LysM}$-cko mice (Fig. 5, O and PP staining of the OB cultures (Fig. 5, Q and R). Taken together, these results suggest that Myo10 suppresses OC formation in a cell-autonomous manner.

Increased expression of Unc5b, RANK, integrin αV and integrin β3 in OC from $Myo10^{m/m}$ mice

To understand how Myo10 negatively regulates OC formation, we examined expression levels of possible Myo10 cargos involved in OC formation. Previous studies have identified numerous Myo10 cargos, including integrin β1,[10] DCC, and neogenin (a DCC family receptor).[9] While integrin αV and β3 are highly expressed in BMMs/OCs, mediating OC migration and formation,[36-38] little DCC or neogenin was detectable in BMMs/OCs (data not shown). Interestingly, Unc5 family netrin-1 receptors were abundant in BMMs (Supplement Fig. 2), and numerous studies have confirmed the importance of Unc5b[24-27] and receptor activator of NF-κB (RANK)[39-41] in OC formation. We thus examined the expression levels of these receptors (Unc5b, RANK, integrin αV and integrin β3) in OCs from control and $Myo10^{m/m}$ mice (Fig. 6, A). All these proteins (Unc5b, RANK, integrin αV and integrin β3) were increased in OCs from $Myo10^{m/m}$ mice (Fig. 6, B-E), in line with the view for an increased OC formation in $Myo10^{m/m}$ mice. Notice that in BMMs without RANKL treatment, Unc5b level was the most abundant one among different family members, but no significant change was detected in the mutant BMMs at the mRNA level

(Supplement Fig. 2). These observations lead us further investigating the distribution pattern and function of Unc5b in BMMs.

Suppression of Unc5b cell surface distribution by Myo10

Cell surface protein biotinylation analysis of BMMs was firstly carried out to examine the distribution patterns of Unc5b. The biotinylated proteins were pulled-down with streptavidin agarose beads and subjected to Western blot with anti-Unc5b antibody. Total protein levels of Unc5b in BMMs without RANKL treatment didn't show significant changes (Fig. 7, A), consistent with unchanged Unc5b mRNA level. We also found more cell surface with less cytoplasmic levels of Unc5b in BMMs from $Myo10^{m/m}$ mice (Fig. 7, A and B), compared to that of $Myo10^{+/+}$ mice. To further study the effect of Myo10 on the subcellular localization of Unc5b, we co-transfected the Flag-Unc5b plasmid with GFP-tagged Full length-Myo10 (FL) or Headless-Myo10 (HL, an isoform which lacks the motor domain)[42] plasmid in Raw 264.7 cells, a macrophage cell line. The GFP plasmid was used as a control. In contrast to control, the presence of FL dramatically distracted Unc5b into the cytoplasm from the plasma membrane (represented by Dil staining) (Fig. 7, C-E), further consolidating the previous data (Fig. 7, A and B). Interestingly, co-transfection with HL recovered Unc5b plasma membrane localization to some extent (Fig. 7, C-E), suggesting a requirement of the motor domain of Myo10 in this event. Next, Flag-Unc5b combined with GFP or GFP-FL-Myo10 plasmids were co-transfected in HEK293T cells and cell surface proteins were biotinylated. The biotinylated proteins were then pulled-down with streptavidin agarose beads and subjected to Western blot with anti-Flag antibody. Again, we found less cell surface with more cytoplasmic levels of Flag-Unc5b expression in GFP-Myo10 co-transfected cells (Fig. 7, F and G), compared to that of GFP co-transfected cells. Together, these results demonstrate a role of Myo10 in suppression of Unc5b cell surface distribution.

Decreased OC formation in $Myo10^{m/m}$ BMMs infected with lentivirus encoding shRNA of Unc5b

To further establish the roles of Unc5b in Myo10 regulated OC formation, we examined the OC formation in $Myo10^{m/m}$ BMMs infected with lentiviruses expressing control or Unc5b-shRNA. The infection efficacy was first checked by fluorescence microscope, which showed that most of the BMMs (>80%) were infected, as represented by GFP expression 4 days after infection (Fig. 8 A). The knockdown efficacy was further confirmed by western blot, which showed markedly reduced protein levels of Unc5b in $Myo10^{m/m}$ BMMs infected with the shUnc5b lentivirus, but not with control shRNA (Fig. 8, B and C). Next we examined the OC formation after control or Unc5b-shRNA lentivirus infection. Concomitantly, the increased OC formation in $Myo10^{m/m}$ mice was suppressed by shUnc5b lentivirus, but not by control shRNA (Fig. 8, D and E). Taken together, these results suggested a critical role of Unc5b in the increase of OC formation in $Myo10^{m/m}$ BMMs.

Increased OC formation in $Myo10^{m/m}$ BMMs in response to netrin-1

Since $Myo10^{m/m}$ BMMs exhibited higher cell surface levels of Unc5b and Unc5b acts as a receptor of netrin-1, we wondered whether netrin-1 could regulate OC formation in $Myo10^{+/+}$ and $Myo10^{m/m}$ mice. Netrin-1 conditioned medium was harvested, whose expression was confirmed by Western blot analysis (Supplement Fig. 3). BMMs from

Myo10$^{+/+}$ and Myo10$^{m/m}$ mice were exposed to 10 ng/ml of M-CSF and 100 ng/ml recombinant RANKL in the presence of control or netrin-1 medium. Results showed that netrin-1 treatment increased OC formation in BMMs from both Myo10$^{+/+}$ and Myo10$^{m/m}$ mice, compared to that of control medium (Fig. 9, A-C), and the increased fold of netrin-1 treated/untreated osteoclastogenesis was higher in Myo10$^{m/m}$ BMMs (Fig. 9, D), suggesting that the increased cell surface distribution of Unc5b in Myo10$^{m/m}$ BMMs might enhanced netrin-1 response. Next we examined netrin-1-Unc5b downstream signaling pathways in pre-OCs by western blot analysis. Results showed that the basal level of p-FAK (Tyr861) in Myo10$^{m/m}$ pre-OCs were higher than that of control cells, in line with the basal increase of Unc5b and osteoclastogenesis in Myo10$^{m/m}$ pre-OCs (Fig. 9, E and F). Upon netrin-1 treatment, even higher levels of p-FAK (Tyr861) and p-Src (Tyr416) were detected in Myo10$^{m/m}$ pre-OCs than those of Myo10$^{+/+}$ pre-OCs (Fig. 9, E-G), suggesting that enhanced netrin-1-Unc5b signaling pathway in the mutant BMMs may lead to the increased osteoclastogenesis. These results support a working model in which Myo10-loss in BMMs promotes osteoclastogenesis likely by the increased cell surface level of Unc5b (Fig. 9, H).

Discussion

Maintenance of normal bone mass depends on the dynamic balance of bone formation and bone resorption. In the present study, we showed that Myo10 loss of function in mice (Myo10$^{m/m}$) decreases trabecular bone mass, which appears to be due in large to the increased bone resorption and OC genesis. Similar phenotypes are also observed in OC-selective Myo10 knockout mice. Unc5b expression levels are elevated in OCs from Myo10$^{m/m}$ mice, and Myo10$^{m/m}$ BMMs exhibited more cell surface distribution of Unc5b, while Unc5b's cell surface distribution in cells overexpressing Myo10 is reduced. Moreover, suppression of Unc5b expression in Myo10$^{m/m}$ BMMs by infection with lentivirus encoding shRNA of Unc5b markedly attenuated RANKL induced OC formation. Finally, increased OC formation was observed in Myo10$^{m/m}$ BMMs in response to netrin-1. These observations suggest that Unc5b acting as active receptors of netrin-1, increasing OC formation that is negatively regulated by Myo10. These results thus identify Myo10 as an important negative regulator of OC formation, bone resorption and bone remodeling.

Out study is the first to show in vivo bone phenotypes of Myo10. Previous work found out that Myo10 and BMP6 receptor ALK6 colocalize in a BMP6-dependent fashion, and Myo10 is required for BMP6-dependent Smad activation in endothelial cells.[11] Also BMP6 can increase osteoblast differentiation of BMSCs through induced phosphorylation and nuclear accumulation of Smad5.[43] But so far no research had established the role of Myo10 in regulating osteoblast differentiation or bone formation. Although we showed unchanged bone formation in Myo10$^{m/m}$ mice, the cell-specific function of Myo10 in bone formation still remains unclear, and the phenotype may due to compensatory mechanisms. Generation of osteoblast-selective Myo10 cKO mice will contribute to clarify the cell-autonomous role of Myo10 in bone formation. A previous study indicates that Myo10 has multiple forms and complete KO Myo10 is semi-lethal.[28] Myo10$^{m/m}$ mouse characterized here was not a null, but a hypomorphic allele, with loss of Myo10 function. As shown in Fig. 1 (F), a large reduction, but not a complete loss of full length Myo10 expression, was observed in cells from Myo10$^{m/m}$ mice by RT-PCR analysis. Besides, we have investigated the expression

levels of Full-length Myo10 and Headless Myo10 in BMMs, and the headless Myo10 was detected at a very low level by RT-PCR but undetectable by Western blot analysis (data not shown). However, it remains possible that there are additional unidentified alternative splicing forms or isoforms whose transcription starting site that skip exon 26 and exon 27 where the KO cassette is inserted. According to RT-PCR analysis of Myo10 expression using primers at different domains (data not shown), $Myo10^{m/m}$ mice did express a truncated form of Myo10, containing the N-terminal head domain, but not the C-terminal regions (e.g., MyTH4 and FERM domains), which are critical regions for binding to Myo10 cargos and microtubule. This is likely due to the insertion of KO cassette that blocked the expression of the gene after exon 26. Thus, whereas our results support the view for a loss of function of full length Myo10 in $Myo10^{m/m}$ mice, it remains possible for a gain of function resulted from a truncated Myo10 N-terminal head domain. These possibilities require further investigation.

As for the influence of Myo10 on osteoclast formation, a previous in vitro study showed that RNAi-mediated suppression of Myo10 led to decreased osteoclast sealing zone perimeter, motility and resorptive capacity.[13] However in our study, bone resorption and osteoclast formation were all increased in $Myo10^{m/m}$ mice, both in vivo and in vitro. Discrepancies between our findings and theirs may be explained by different culture protocols. In their study, siRNAs were transfected on day 4 of osteoclast differentiation, and Myo10 mRNA level, protein level, as well as osteoclast motility and resorptive activity were assayed 2 to 4 days post-transfection. Under our protocol, mature osteoclast formed about 4 to 5 days after induced for differentiation, and many of them underwent apoptosis at day 6. The results they found may not solely due to Myo10 knockdown by siRNA. Osteoclast timeline may also contribute to the difference. Another recent study showed lentiviral knockdown of Myo10 inhibited osteoclast fusion, migration and formation of tunneling nanotubes (TNT).[14] But there were still several discrepancies in their study. They didn't find significant difference in the average size of the resorption pit or the ability to adhere in osteoclast with Myo10 knockdown. Neither did they detect any changes in the MAPK signaling pathways, which is important for the regulation of osteoclast differentiation.[44] Also no difference was found in the expression of m-sec gene, which is crucial for TNT formation. All these discrepancies may not reflect the actual in vivo role of Myo10 in regulating osteoclast activity. While in our study, the increased resorption and osteoclast formation in $Myo10^{m/m}$ mice was further confirmed in OC-selective Myo10 knockout mice, revealing the cell-autonomous manner of Myo10 regulating osteoclast formation.

Although the expression level of Unc5b was increased in OCs from $Myo10^{m/m}$ mice, no significant difference was observed in BMMs between $Myo10^{+/+}$ and $Myo10^{m/m}$ mice. At the same time, increased expression of Unc5b was accompanied by increased expressions of RANK, integrin αV and integrin β3, suggesting that these changes might be the consequence, but not the cause, of increased OC formation. Although a previous study indicates that Myo10 participates in an amplification loop for BMP signaling,[11] no evidence has supported Myo10's function in regulating transcription. Myo10 is an unconventional MyTH4-FERM containing myosin, which mainly functions in binding to different cargos. We thus speculate that Unc5b might act as a Myo10 cargo. While our observations of altered Unc5b distribution in $Myo10^{m/m}$ BMMs and in Myo10

overexpression conditions support this view, it needs further investigation. Also further studies are necessary to address the effects of Unc5b lentiviral knockdown on bone mass.

Collectively, this study demonstrated an unrecognized function of Myo10 in negatively regulating OC formation and bone remodeling. The effects were through altered cell surface distribution of Unc5b to regulate osteoclast formation and differentiation.

Supplementary Material

Refer to Web version on PubMed Central for supplementary material.

Acknowledgments

This work was supported in part by grants from National Institutes of Health (AG051773) and VA (BX000838). We thank members of Dr. Xiong and Mei laboratories for helpful discussions and suggestions. We thank Dr. Xiaojuan Zhu from Northeast Normal University for providing Unc5b shRNAs. We thank The University of Alabama μCT Core for μCT analysis.

References

1. Raggatt LJ, Partridge NC. Cellular and molecular mechanisms of bone remodeling. J Biol Chem. 2010;285(33):25103–8. [PubMed: 20501658]
2. Boyle WJ, Simonet WS, Lacey DL. Osteoclast differentiation and activation. Nature. 2003;423(6937):337–42. [PubMed: 12748652]
3. Zhu XJ, Wang CZ, Dai PG, et al. Myosin X regulates netrin receptors and functions in axonal path-finding. Nat Cell Biol. 2007;9(2):184–92. [PubMed: 17237772]
4. Kerber ML, Cheney RE. Myosin-X: a MyTH-FERM myosin at the tips of filopodia. J Cell Sci. 2011;124(Pt 22):3733–41. [PubMed: 22124140]
5. Yu H, Lai M, Guo Y, et al. Myo10 is required for neurogenic cell adhesion and migration. In Vitro Cell Dev Biol Anim. 2015;51(4):400–7. [PubMed: 25491426]
6. Lai M, Guo Y, Ma J, et al. Myosin X regulates neuronal radial migration through interacting with N-cadherin. Front Cell Neurosci. 2015;9:326. [PubMed: 26347613]
7. Woolner S, O'Brien LL, Wiese C, Bement WM. Myosin-10 and actin filaments are essential for mitotic spindle function. J Cell Biol. 2008;182(1):77–88. [PubMed: 18606852]
8. Cao R, Chen J, Zhang X, et al. Elevated expression of myosin X in tumours contributes to breast cancer aggressiveness and metastasis. British Journal Of Cancer. 2014;111(3):539–50. [PubMed: 24921915]
9. Liu Y, Peng Y, Dai PG, Du QS, Mei L, Xiong WC. Differential regulation of myosin X movements by its cargos, DCC and neogenin. J Cell Sci. 2012;125(Pt 3):751–62. [PubMed: 22349703]
10. Zhang H, Berg JS, Li Z, et al. Myosin-X provides a motor-based link between integrins and the cytoskeleton. Nat Cell Biol. 2004;6(6):523–31. [PubMed: 15156152]
11. Pi X, Ren R, Kelley R, et al. Sequential roles for myosin-X in BMP6-dependent filopodial extension, migration, and activation of BMP receptors. J Cell Biol. 2007;179(7):1569–82. [PubMed: 18158328]
12. Kwon M, Bagonis M, Danuser G, Pellman D. Direct Microtubule-Binding by Myosin-10 Orients Centrosomes toward Retraction Fibers and Subcortical Actin Clouds. Dev Cell. 2015;34(3):323–37. [PubMed: 26235048]
13. McMichael BK, Cheney RE, Lee BS. Myosin X regulates sealing zone patterning in osteoclasts through linkage of podosomes and microtubules. J Biol Chem. 2010;285(13):9506–15. [PubMed: 20081229]
14. Tasca A, Astleford K, Lederman A, et al. Regulation of Osteoclast Differentiation by Myosin X. Sci Rep. 2017;7(1):7603. [PubMed: 28790434]

15. Low K, Culbertson M, Bradke F, Tessier-Lavigne M, Tuszynski MH. Netrin-1 is a novel myelin-associated inhibitor to axon growth. J Neurosci. 2008;28(5):1099–108. [PubMed: 18234888]
16. Bradford D, Cole SJ, Cooper HM. Netrin-1: diversity in development. Int J Biochem Cell Biol. 2009;41(3):487–93. [PubMed: 18455953]
17. Castets M, Mehlen P. Netrin-1 role in angiogenesis: to be or not to be a pro-angiogenic factor? Cell Cycle. 2010;9(8):1466–71. [PubMed: 20372055]
18. Hata K, Kaibuchi K, Inagaki S, Yamashita T. Unc5B associates with LARG to mediate the action of repulsive guidance molecule. J Cell Biol. 2009;184(5):737–50. [PubMed: 19273616]
19. Finci LI, Kruger N, Sun X, et al. The crystal structure of netrin-1 in complex with DCC reveals the bifunctionality of netrin-1 as a guidance cue. Neuron. 2014;83(4):839–49. [PubMed: 25123307]
20. Lu X, Le Noble F, Yuan L, et al. The netrin receptor UNC5B mediates guidance events controlling morphogenesis of the vascular system. Nature. 2004;432(7014):179–86. [PubMed: 15510105]
21. Tang X, Jang SW, Okada M, et al. Netrin-1 mediates neuronal survival through PIKE-L interaction with the dependence receptor UNC5B. Nat Cell Biol. 2008;10(6):698–706. [PubMed: 18469807]
22. Arakawa H p53, apoptosis and axon-guidance molecules. Cell Death Differ. 2005;12(8):1057–65. [PubMed: 15818407]
23. Larrivee B, Freitas C, Trombe M, et al. Activation of the UNC5B receptor by Netrin-1 inhibits sprouting angiogenesis. Genes Dev. 2007;21(19):2433–47. [PubMed: 17908930]
24. Mediero A, Ramkhelawon B, Wilder T, et al. Netrin-1 is highly expressed and required in inflammatory infiltrates in wear particle-induced osteolysis. Ann Rheum Dis. 2016;75(9):1706–13. [PubMed: 26452536]
25. Mediero A, Wilder T, Ramkhelawon B, Moore KJ, Cronstein BN. Netrin-1 and its receptor Unc5b are novel targets for the treatment of inflammatory arthritis. FASEB J. 2016;30(11):3835–44. [PubMed: 27502509]
26. Mediero A, Mazumder A, Cronstein B. Netrin-1 and Its Receptors Unc5b and DCC May be Useful Targets for Preventing Multiple Myeloma Bone Lesions. Blood. 2015;126(23).
27. Mediero A, Ramkhelawon B, Perez-Aso M, Moore KJ, Cronstein BN. Netrin-1 is a critical autocrine/paracrine factor for osteoclast differentiation. J Bone Miner Res. 2015;30(5):837–54. [PubMed: 25483983]
28. Heimsath EG Jr., Yim YI, Mustapha M, Hammer JA, Cheney RE. Myosin-X knockout is semi-lethal and demonstrates that myosin-X functions in neural tube closure, pigmentation, hyaloid vasculature regression, and filopodia formation. Sci Rep. 2017;7(1):17354. [PubMed: 29229982]
29. Zhou Z, Xie J, Lee D, et al. Neogenin regulation of BMP-induced canonical Smad signaling and endochondral bone formation. Dev Cell. 2010;19(1):90–102. [PubMed: 20643353]
30. Xiong L, Jung JU, Wu H, et al. Lrp4 in osteoblasts suppresses bone formation and promotes osteoclastogenesis and bone resorption. Proc Natl Acad Sci U S A. 2015;112(11):3487–92. [PubMed: 25733894]
31. Bouxsein ML, Boyd SK, Christiansen BA, Guldberg RE, Jepsen KJ, Muller R. Guidelines for assessment of bone microstructure in rodents using micro-computed tomography. J Bone Miner Res. 2010;25(7):1468–86. [PubMed: 20533309]
32. Cui S, Xiong F, Hong Y, et al. APPswe/Abeta regulation of osteoclast activation and RAGE expression in an age-dependent manner. J Bone Miner Res. 2011;26(5):1084–98. [PubMed: 21542009]
33. Dempster DW, Compston JE, Drezner MK, et al. Standardized nomenclature, symbols, and units for bone histomorphometry: a 2012 update of the report of the ASBMR Histomorphometry Nomenclature Committee. J Bone Miner Res. 2013;28(1):2–17. [PubMed: 23197339]
34. Cole SR, Ashman LK, Ey PL. Biotinylation: an alternative to radioiodination for the identification of cell surface antigens in immunoprecipitates. Mol Immunol. 1987;24(7):699–705. [PubMed: 3309626]
35. Clausen BE, Burkhardt C, Reith W, Renkawitz R, Forster I. Conditional gene targeting in macrophages and granulocytes using LysMcre mice. Transgenic Res. 1999;8(4):265–77. [PubMed: 10621974]

36. Nakamura I, Pilkington MF, Lakkakorpi PT, et al. Role of alpha(v)beta(3) integrin in osteoclast migration and formation of the sealing zone. J Cell Sci. 1999;112 (Pt 22):3985–93. [PubMed: 10547359]

37. Duong LT, Lakkakorpi P, Nakamura I, Rodan GA. Integrins and signaling in osteoclast function. Matrix Biol. 2000;19(2):97–105. [PubMed: 10842093]

38. Nakamura I, Duong LT, Rodan SB, Rodan GA. Involvement of alpha(v)beta3 integrins in osteoclast function. J Bone Miner Metab. 2007;25(6):337–44. [PubMed: 17968485]

39. Li J, Sarosi I, Yan XQ, et al. RANK is the intrinsic hematopoietic cell surface receptor that controls osteoclastogenesis and regulation of bone mass and calcium metabolism. Proc Natl Acad Sci U S A. 2000;97(4):1566–71. [PubMed: 10677500]

40. Kim H, Choi HK, Shin JH, et al. Selective inhibition of RANK blocks osteoclast maturation and function and prevents bone loss in mice. J Clin Invest. 2009;119(4):813–25. [PubMed: 19258703]

41. Xia WF, Tang FL, Xiong L, et al. Vps35 loss promotes hyperresorptive osteoclastogenesis and osteoporosis via sustained RANKL signaling. J Cell Biol. 2013;200(6):821–37. [PubMed: 23509071]

42. Raines AN, Nagdas S, Kerber ML, Cheney RE. Headless Myo10 is a negative regulator of full-length Myo10 and inhibits axon outgrowth in cortical neurons. J Biol Chem. 2012;287(30):24873–83. [PubMed: 22661706]

43. Ebisawa T, Tada K, Kitajima I, et al. Characterization of bone morphogenetic protein-6 signaling pathways in osteoblast differentiation. J Cell Sci. 1999;112 (Pt 20):3519–27. [PubMed: 10504300]

44. Lee K, Chung YH, Ahn H, Kim H, Rho J, Jeong D. Selective Regulation of MAPK Signaling Mediates RANKL-dependent Osteoclast Differentiation. Int J Biol Sci. 2016;12(2):235–45. [PubMed: 26884720]

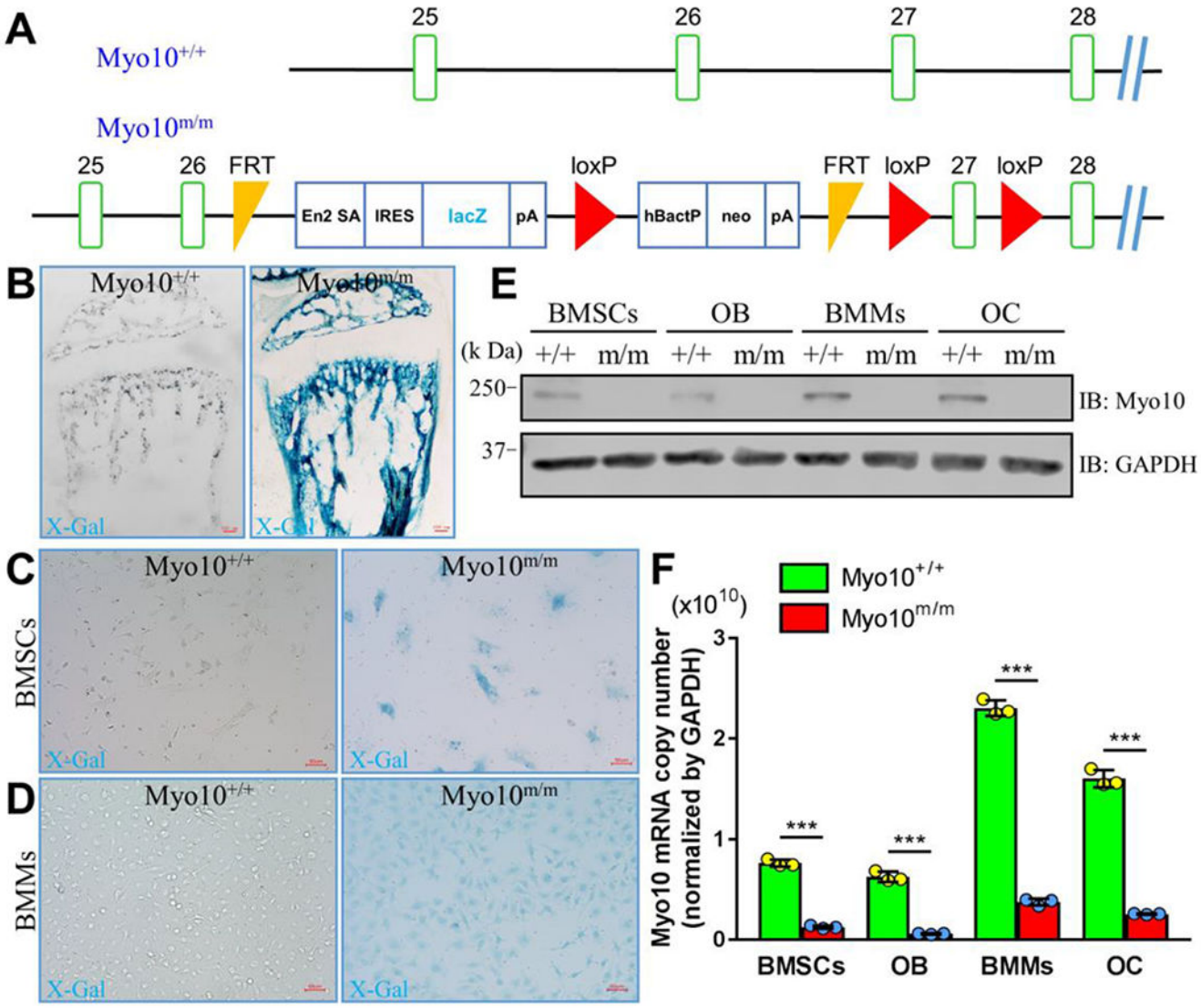

Fig. 1.

Characterization of the Myo10$^{m/m}$ mice. (A) Illustration for the generation of Myo10$^{m/m}$ mice. (B-D) Detection of enzymatic LacZ activity in femurs of neonatal (P15) Myo10$^{m/m}$ mice, but not Myo10$^{+/+}$ mice (B) and in purified BMSCs (C) and BMMs (D) from Myo10$^{m/m}$ mice, but not Myo10$^{+/+}$ mice. Bars, 100 μm in B, 50 μm in C and D. In C and D, over 90% of cells (BMSCs and BMMs) were positive for LacZ activity. (E) Western blot analysis of Myo10 protein levels in BMSCs, OB, BMMs and OC derived from Myo10$^{+/+}$ and Myo10$^{m/m}$ mice. (F) Real-Time PCR analysis of the mRNA levels of Myo10 in BMSCs, OB, BMMs and OC derived from Myo10$^{+/+}$ and Myo10$^{m/m}$ mice. The values are normalized by GAPDH. Mean ± SD values are from three different experiments. ***p <0.001, significant difference.

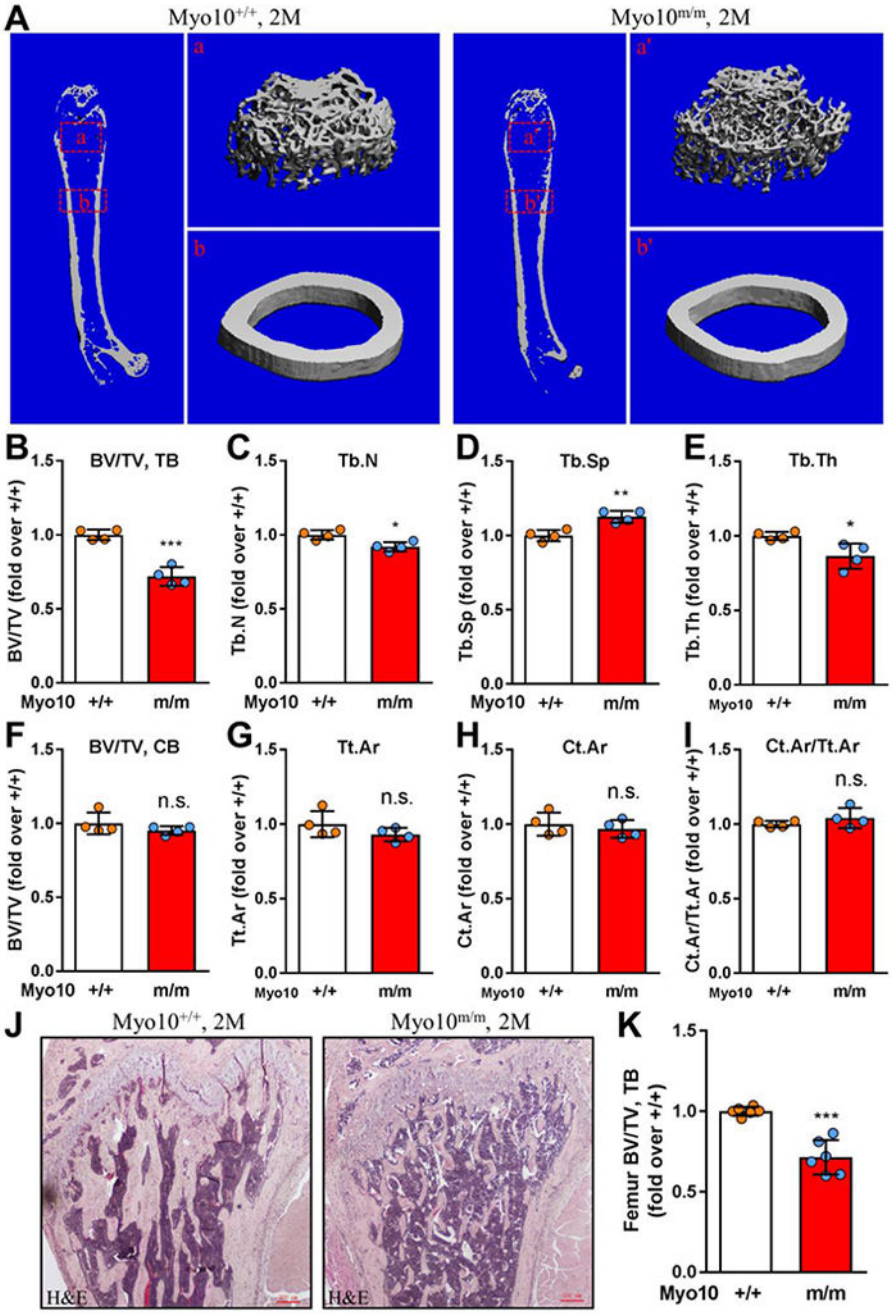

Fig. 2.

Osteoporotic deficits in young adult Myo10$^{m/m}$ mice. (A-I) The μCT analysis of femurs from 2-month-old Myo10$^{+/+}$ and Myo10$^{m/m}$ littermates. Four different male mice of each genotype were examined blindly. Representative images are shown in A. The 3D images shown on the right (a, a', b and b') were derived from the marked corresponding regions of the femurs shown on the left. Quantitative analysis (mean ± SD, n=4) are presented in B-I. Note that trabecular bone volumes over total volumes (BV/TV) (B), trabecular bone numbers (Tb.N) (C), trabecular separation (Tb.Sp) (D) and trabecular thickness (Tb.Th) (E) were all deficient in Myo10$^{m/m}$ as compared to the control littermates. *p <0.05, **p <0.01,

***p <0.001, significant difference. The cortical BV/TV (F), total cross-sectional area (Tt.Ar) (G), cortical bone area (Ct.Ar) (H) and cortical bone area fraction (Ct.Ar/Tt.Ar) (I) in Myo10$^{m/m}$ mice appeared to be normal. (J and K) H&E staining analysis of femur sections from 2-month-old Myo10$^{+/+}$ and Myo10$^{m/m}$ littermates. Representative images are shown in J. Bars, 200 μm. Quantitative analysis (mean ± SD, n=6) are presented in K. ***p <0.001, significant difference.

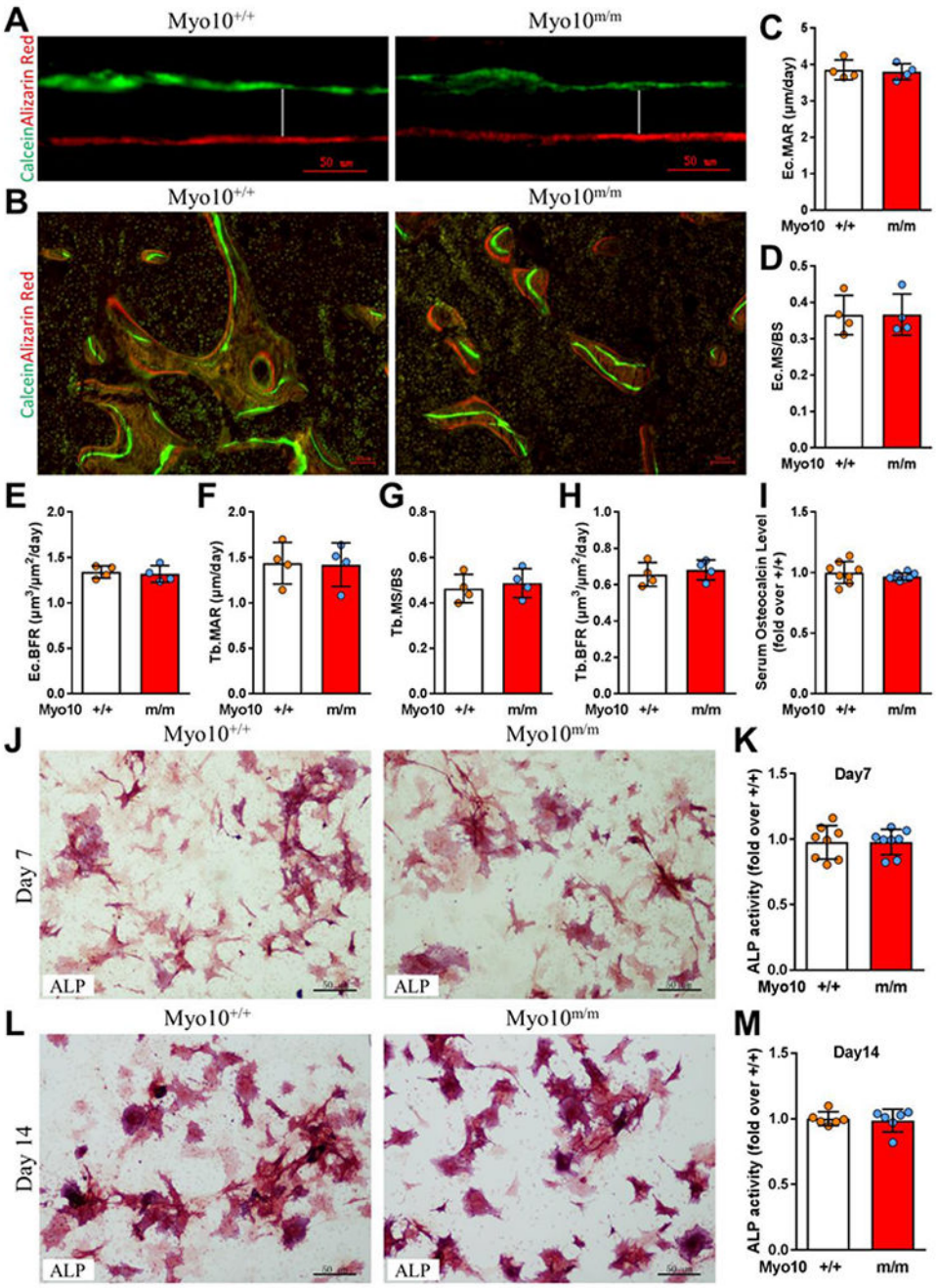

Fig. 3.

No change of bone formation in Myo10$^{m/m}$ mice. (A-H) No change of endocortical and trabecular bone formation in Myo10$^{m/m}$ mice detected by dynamic histomorphometric measurements of calcein green and alizarin red double-fluorescent-labeled femurs. Four different male mice of each genotype were examined. Representative images of histological sections showing calcein green and alizarin red double-fluorescent-labeling of endocortical bone in femur mid diaphysis and trabecular bone of Myo10$^{+/+}$ and Myo10$^{m/m}$ mice are shown in A and B, respectively. Bars, 50 μm. Quantitative analysis (mean ± SD, n=4) of endocortical as well as trabecular mineral apposition rate (Ec. MAR (C) and Tb. MAR (F)),

mineral surface / bone surface (Ec. MS/BS (D) and Tb. MS/BS (G)), and bone formation rate (Ec. BFR (E) and Tb. BFR (H)) are presented. p >0.05, no significant difference. (I) Unchanged serum levels of osteocalcin in 2-month-old $Myo10^{+/+}$ and $Myo10^{m/m}$ mice measured by ELISA assays (see Materials and methods). The values of mean ± SD from eight different male mice of each genotype are shown. p >0.05, no significant difference. (J-M) Unchanged in vitro OB differentiation were detected by alkaline phosphatase (ALP) staining analysis of $Myo10^{+/+}$ and $Myo10^{m/m}$ OB cultures. Representative images of ALP staining at day 7 and 14 cultures are shown in J and L, respectively. Bars, 50 μm. Quantitative analysis of ALP activity (ALP positive area/total area, normalized to $Myo10^{+/+}$ mice) at day 7 and 14 are presented in K and M (mean ± SD, n=8 and n=6, respectively). p >0.05, no significant difference.

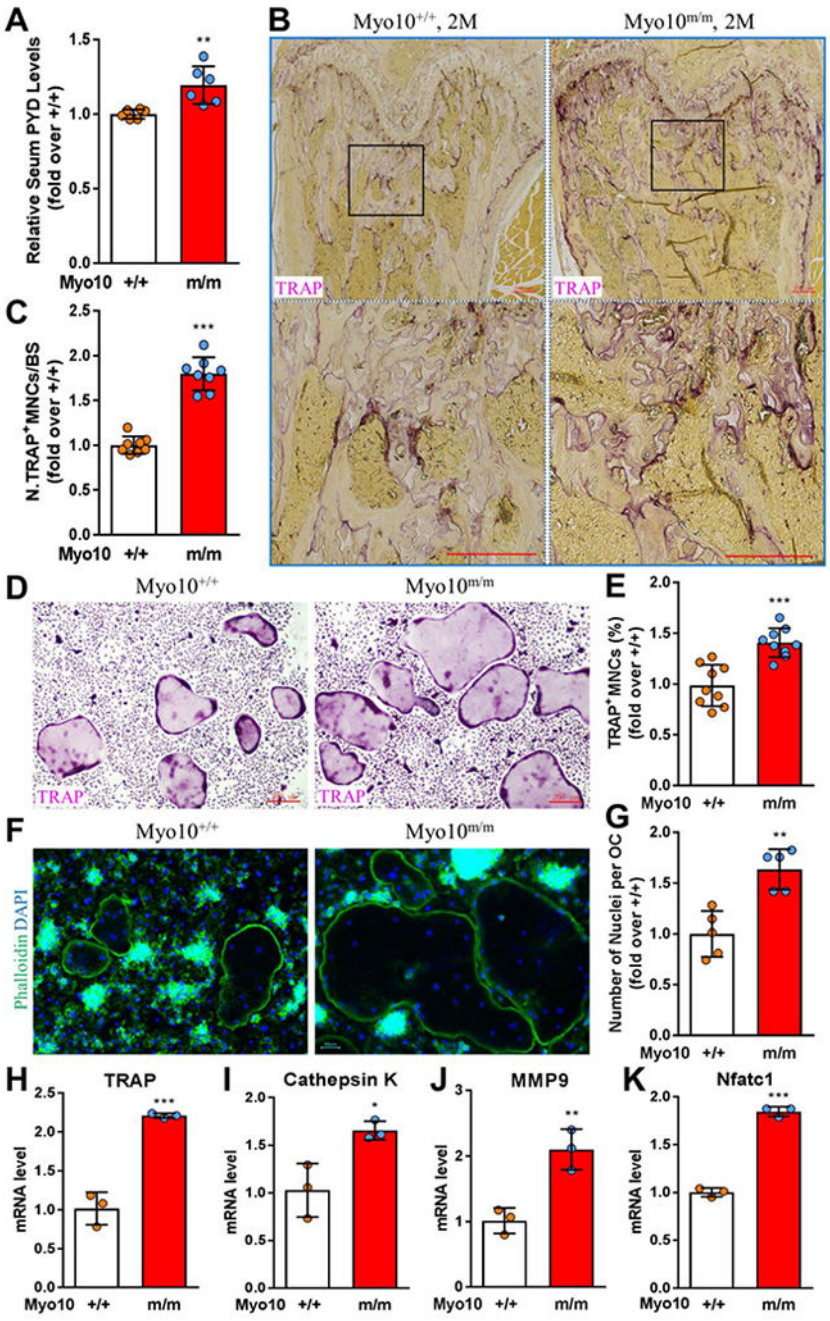

Fig. 4.

Increased bone resorption and OC formation in Myo10$^{m/m}$ mice. (A) Measurement of serum levels of PYD in 2-month-old Myo10$^{+/+}$ and Myo10$^{m/m}$ mice by RIA assays. Six different male mice of each genotype were measured and the values of mean ± SD are shown. $^{**}p$ <0.01, significant difference. (B and C) TRAP staining analysis of femur sections from 2-month-old Myo10$^{+/+}$ and Myo10$^{m/m}$ littermates. Eight different male mice of each genotype were examined. Representative images are shown in B. Images marked with black squares were amplified and shown in the bottom. Bars, 200 μm. The quantitative analysis of TRAP+ cells per unit bone surface (normalized to Myo10$^{+/+}$ mice) is presented in C. $^{***}p$ <0.001,

significant difference. (D-G) TRAP staining (D and E) and phalloidin immunofluorescence staining (F and G) analysis of OC. BMMs from $Myo10^{+/+}$ and $Myo10^{m/m}$ mice were treated with 10 ng/ml M-CSF and 100 ng/ml recombinant RANKL for 5 days to induce OC. Representative images are shown in D and F. Bars, 200 μm in D, 50 μm in F. Quantitative analysis of the $TRAP^{+}$ multinuclei cell (MNCs) density and nuclei numbers per OC were presented in E and G (mean ± SD, n=9 in E and n=5 in G, respectively). $^{**}p < 0.01$, $^{***}p < 0.001$, significant difference. (H-K) Real-Time PCR analysis of the mRNA levels of TRAP (H), Cathepsin K (I), MMP9 (J) and Nfatc1 (K) in OC cultures. The values are normalized to GAPDH and showed in relative to $Myo10^{+/+}$ mice. Mean ± SD values from three different experiments were shown. $^{*}p < 0.05$, $^{**}p < 0.01$, $^{***}p < 0.001$, significant difference.

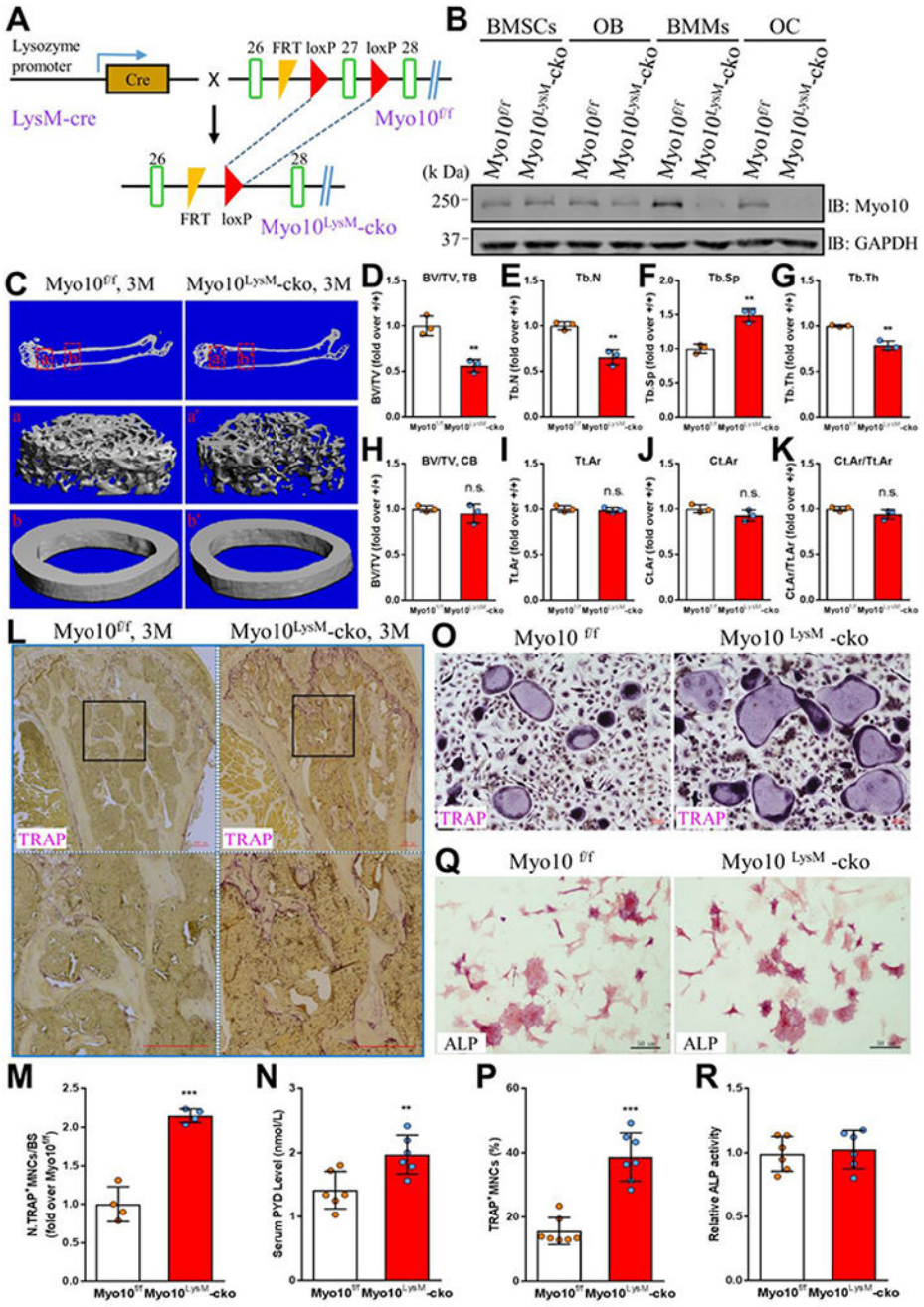

Fig. 5.

Similar osteoporotic deficit with elevated bone resorption and OC formation in OC-selective Myo10 knockout mice. (A) Illustration of breeding strategies for generation of $Myo10^{LysM}$-cko mice. (B) Western blot analysis of Myo10 protein levels in BMSCs, OB, BMMs and OC derived from $Myo10^{f/f}$ and $Myo10^{LysM}$-cko mice. (C-K) The μCT analysis of femurs from 3-month-old $Myo10^{f/f}$ and $Myo10^{LysM}$-cko littermates. Three different male mice of each genotype were examined blindly. Representative images are shown in C. Quantitative analysis (mean ± SD, n=3) are presented in D-K. Note that trabecular bone volumes over total volumes (BV/TV) (D), trabecular bone numbers (Tb.N) (E), trabecular separation

(Tb.Sp) (F) and trabecular thickness (Tb.Th) (G) were all deficient in $Myo10^{LysM}$-cko as compared to the control littermates. $^{**}p < 0.01$, significant difference. The cortical BV/TV (H), total cross-sectional area (Tt.Ar) (I), cortical bone area (Ct.Ar) (J) and cortical bone area fraction (Ct.Ar/Tt.Ar) (K) in $Myo10^{LysM}$-cko mice appeared to be normal. (L-M) TRAP staining analysis of femur sections from 3-month-old $Myo10^{f/f}$ and $Myo10^{LysM}$-cko littermates. Representative images are shown in L. Images marked with black squares were amplified and shown in the bottom. Bars, 200 μm. Quantitative analysis (mean ± SD, n=4) of TRAP+ cells per unit bone surface (normalized to $Myo10^{f/f}$ mice) is presented in M. $^{***}p < 0.001$, significant difference. (N) Measurement of serum levels of PYD in 3-month-old $Myo10^{f/f}$ and $Myo10^{LysM}$-cko mice by RIA assays. Six different male mice of each genotype were measured and the values of mean ± SD are shown. $^{**}p < 0.01$, significant difference. (O and P) TRAP staining analysis of OC derived from $Myo10^{f/f}$ and $Myo10^{LysM}$-cko mice. Representative images are shown in O. Bars, 50 μm. Quantitative analysis (mean ± SD, n=6) of the $TRAP^{+}$ multi-nuclei cell (MNCs) density are presented in P. $^{***}p < 0.001$, significant difference. (Q and R) ALP staining analysis of OB cultures derived from $Myo10^{f/f}$ and $Myo10^{LysM}$-cko mice. Representative images are shown in Q. Bars, 50 μm. Quantitative analysis (mean ± SD, n=6) of ALP activity (ALP positive area/total area, normalized to $Myo10^{f/f}$ mice) are presented in R. $p > 0.05$, no significant difference.

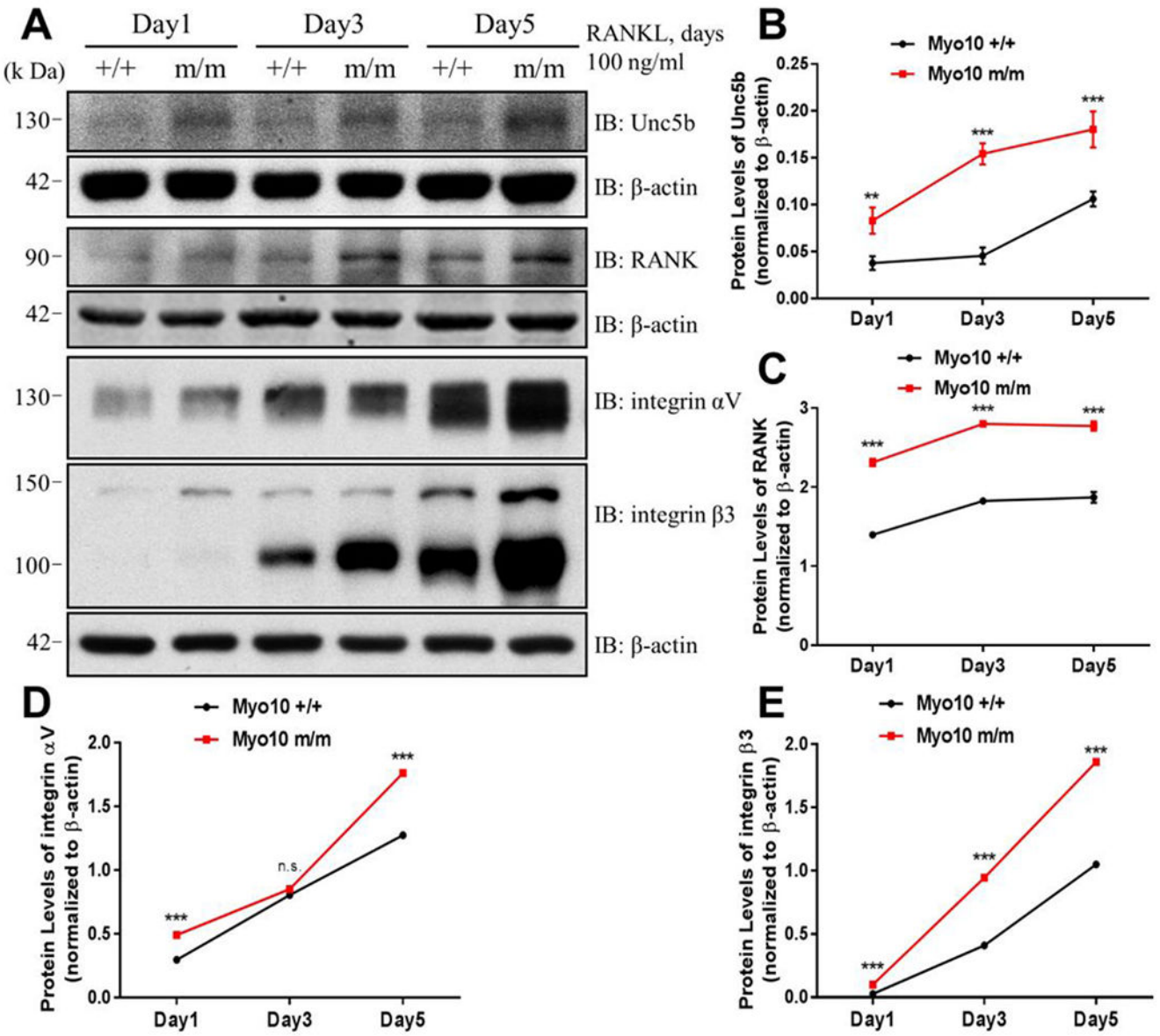

Fig. 6.

Increased expression of Unc5b, RANK, integrin αV and integrin β3 in OC from Myo10$^{m/m}$ mice. (A) Western blot analysis of Unc5b, RANK, integrin αV and integrin β3 protein levels in OC derived from Myo10$^{+/+}$ and Myo10$^{m/m}$ mice under treatment of RANKL for indicated days. (B-E) Quantification analysis (mean ± SD, n=3) of Unc5b (B), RANK (C), integrin αV (D) and integrin β3 (E) protein levels are presented. ** p <0.01, *** p <0.001, significant difference.

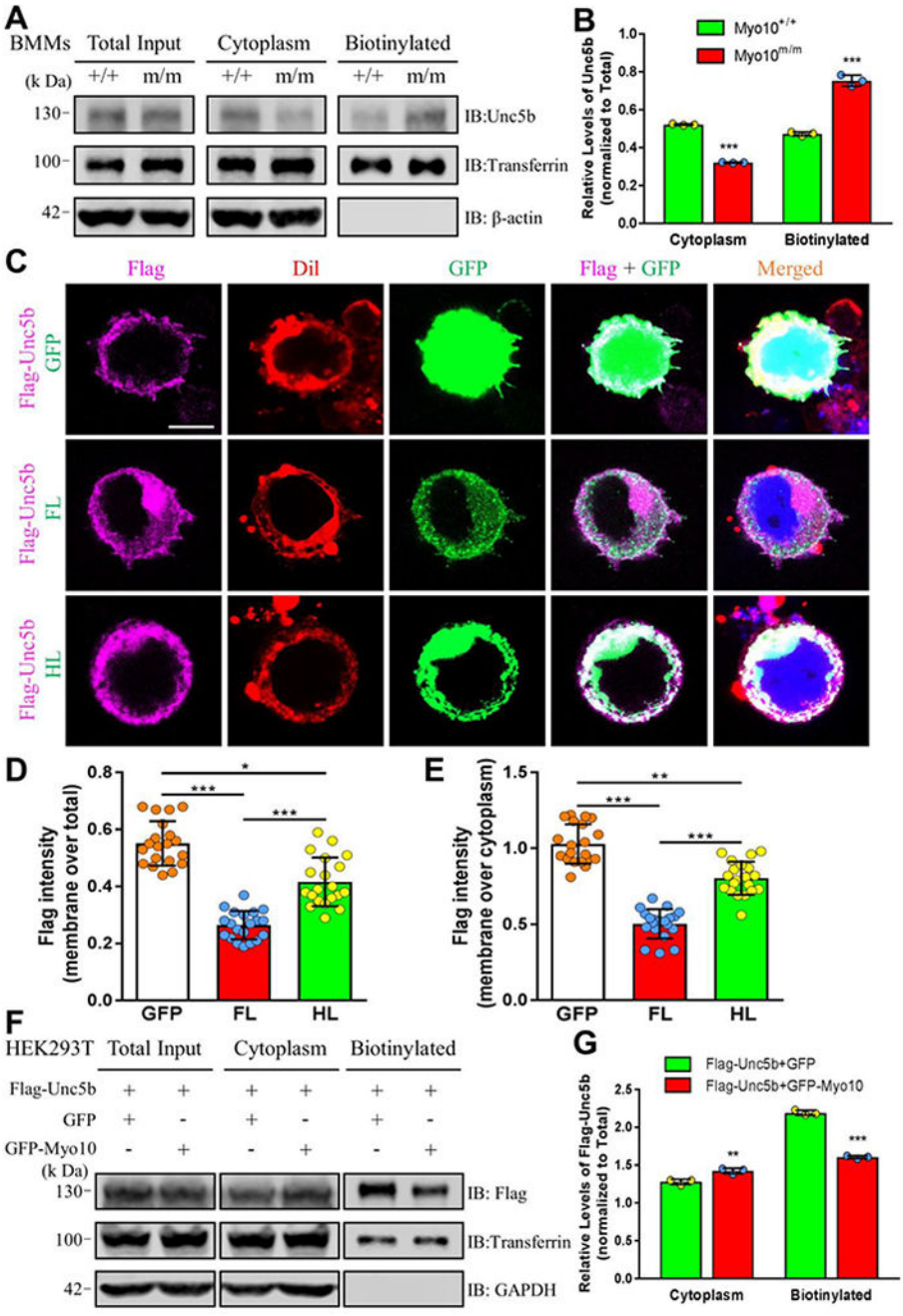

Fig. 7.

Suppression of Unc5b cell surface distribution by Myo10. (A and B) Increased cell surface level of Unc5b in Myo10$^{m/m}$ BMMs by cell surface biotinylation assay (see Materials and Methods). Representative blots are shown in A. Quantitative analysis (mean ± SD, n=3) is presented in B. ***p <0.001, significant difference. (C-G) Decreased cell surface distribution of Unc5b in cells overexpressing Myo10. (C) Immunofluorescence staining analysis of exogenous Unc5b distribution in RAW264.7 cells transfected with Flag-tagged Unc5b combined with GFP, GFP-tagged Full-length Myo10 (FL) or Headless Myo10 (HL) plasmids. Bars, 5 μm. Quantitative analysis (mean ± SD, n=20) of relative fluorescent

intensity of Flag-Unc5b on the plasma membrane versus total or cytoplasm are shown in D and E. *p <0.05, **p <0.01, ***p <0.001, significant difference. (F) Cell surface biotinylation analysis of HEK293T cells transfected with indicated plasmids. Representative blots are shown. Quantitative analysis (mean ± SD, n=3) is presented in G. **p <0.01, ***p <0.001, significant difference.

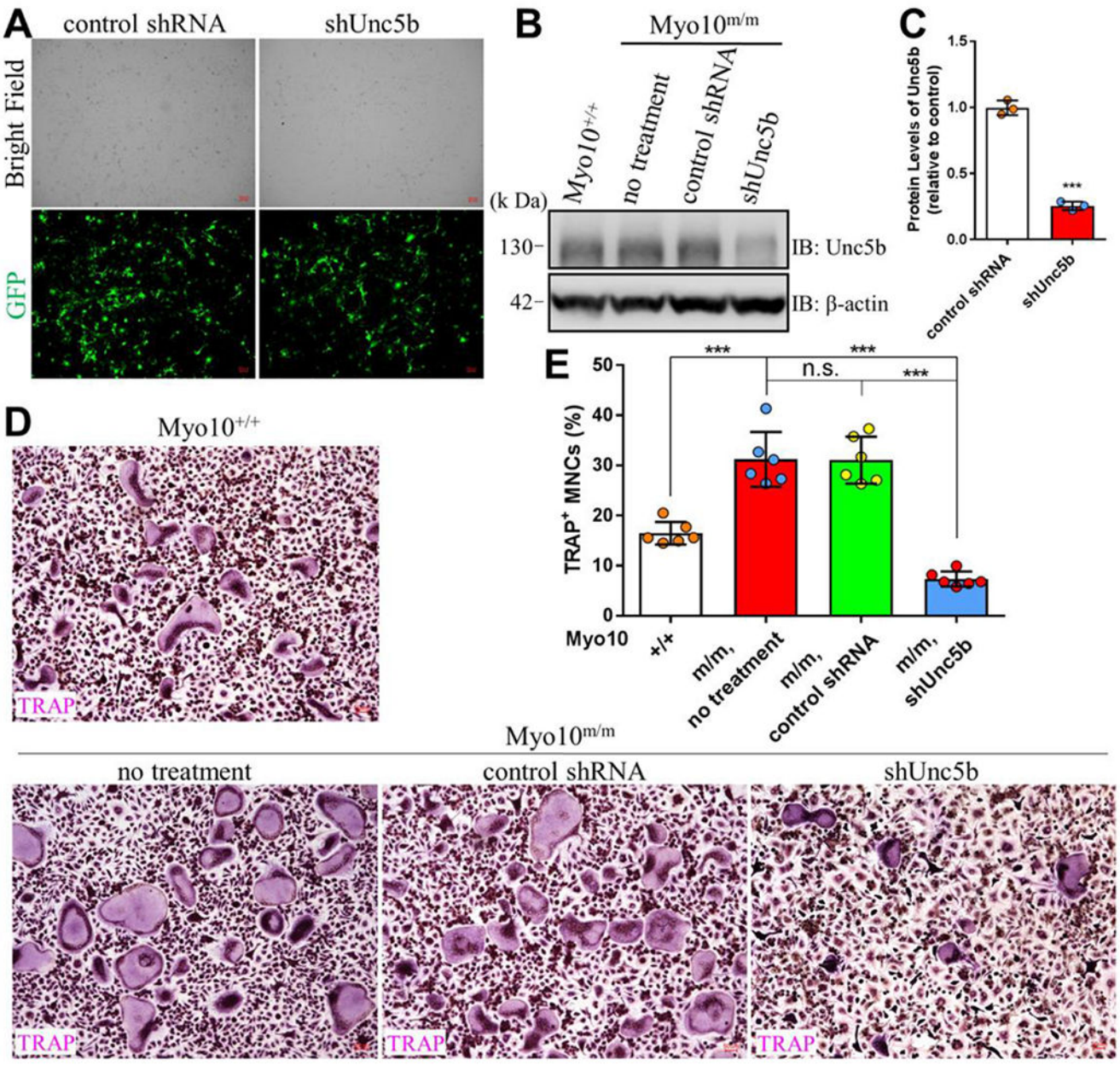

Fig. 8.

Decreased OC formation in Myo10$^{m/m}$ BMMs infected with lentivirus encoding shRNA of Unc5b. (A) The infection efficacy of lentivirus expressing control and Unc5b-shRNA in Myo10$^{m/m}$ BMMs. Representative images are shown. Bars, 50 μm. (B and C) Western blot analysis of Unc5b protein levels in BMMs infected with lentivirus expressing control or Unc5b-shRNA. Representative blots are shown in B. Quantitative analysis (mean ± SD, n=3) is presented in C. (D and E) TRAP staining analysis of OC derived from BMMs infected with lentivirus expressing control or Unc5b-shRNA. Representative images are shown in D. Bars, 50 μm. Quantitative analysis (mean ± SD, n=6) of the TRAP^{+} multinuclei cell (MNCs) density are presented in E. ***p <0.001, significant difference.

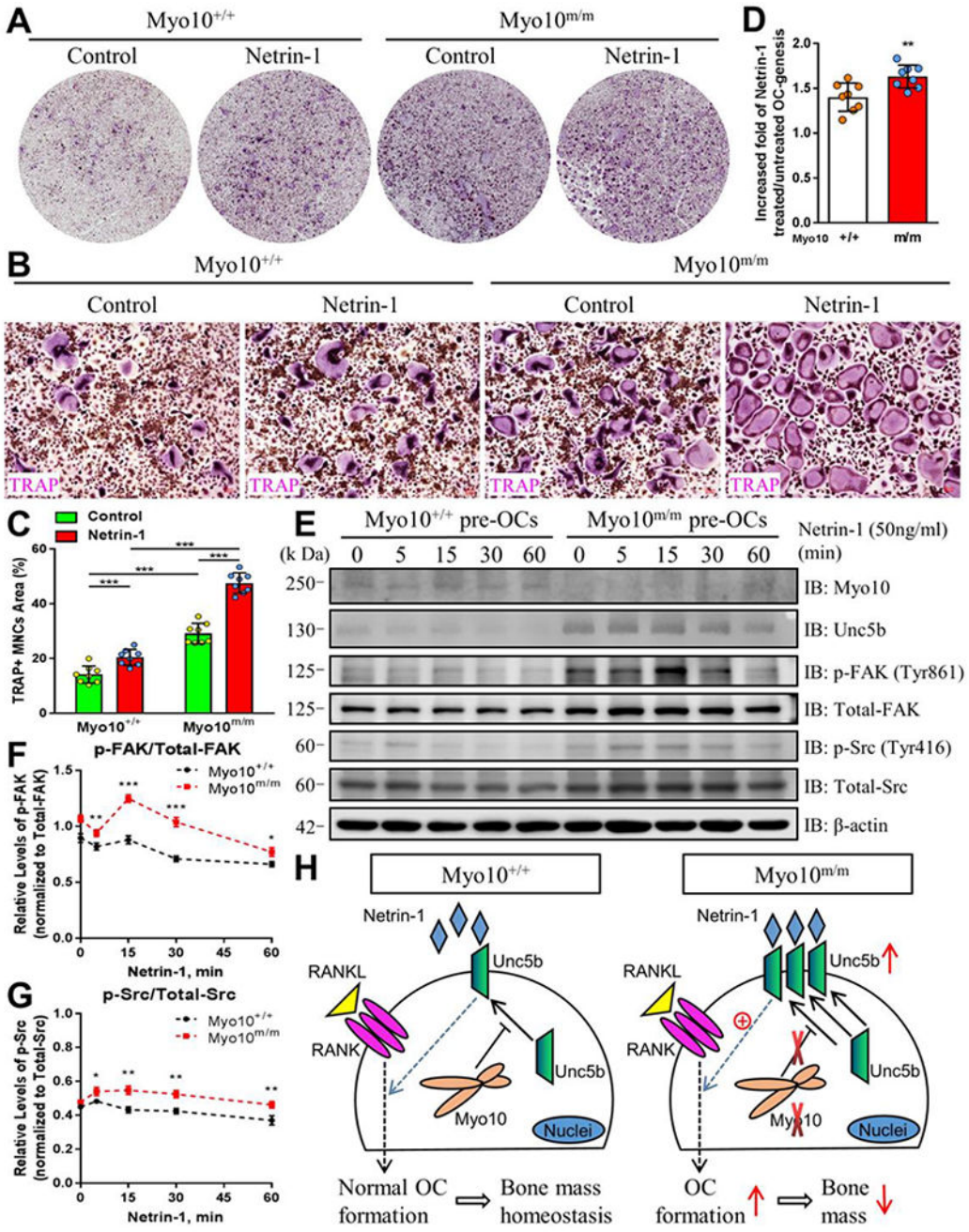

Fig. 9.

Increased OC formation in Myo10$^{m/m}$ BMMs in response to netrin-1. (A-D) TRAP staining analysis of OC derived from Myo10$^{+/+}$ and Myo10$^{m/m}$ mice in the presence of control or netrin-1 medium. Representative images are shown in A and B. Bars, 50 μm. Quantitative analysis (mean ± SD, n=8) of the TRAP^{+} multinuclei cell (MNCs) density are presented in C and D. $^{**}p < 0.01$, $^{***}p < 0.001$, significant difference. (E-G) Western blot analysis of netrin-1-Unc5b downstream signaling pathways in Myo10$^{+/+}$ and Myo10$^{m/m}$ pre-OCs. BMMs from Myo10$^{+/+}$ and Myo10$^{m/m}$ mice were treated with 10 ng/ml M-CSF and 100 ng/ml recombinant RANKL for 2 days, and the pre-OCs were treated with 50 ng/ml

recombinant netrin-1 for indicated time. Representative blots are shown in E. Quantitative analysis (mean ± SD, n=3) of p-FAK/Total-FAK and p-Src/Total-Src protein levels are presented in F and G. *p <0.05, **p <0.01, ***p <0.001, significant difference. (H) Illustration of a working model in which Myo10 negatively regulating OC formation by attenuating Unc5b targeting to the cell surface, inhibiting netrin-1-Unc5b signaling and function during OC genesis.

Table 1.

List of Real-Time PCR Primers Used in This Study

Target	Forward: 5′-3′	Reverse: 5′-3′
GAPDH	AAGGTCATCCCAGAGCTGAA	CTGCTTCACCACCTTCTTGA
Myo10	GACGCCGTGTCTGTCTACAA	CACAGAGCGTGTGGTGCTAT
TRAP	TACCTGTGTGGACATGACC	CAGATCCATAGTGAAACCGC
Cathepsin K	TGTATAACGCCACGGCAAA	GGTTCACATTATCACGGTCACA
MMP9	TCCAGTACCAAGACAAAGCCTA	TTGCACTGCACGGTTGAA
Nfatc1	CAACGCCCTGACCACCGATAG	GGGAAGTCAGAAGTGGGTGGA
Unc5a	CGCAACTGTACCAGTGACCTCT	TTGCGGCAGTAGATGAGGACGA
Unc5b	GGACAGTTACCACAACCTACGC	CTGCCATTCCAGACGTGGTAGA
Unc5c	ACTCAATGGCGGCTTTCAGCCT	GGTCCAGAATTGGAGAGTTGGTC
Unc5d	CACCTGTATGGCAGCCAACATC	CGTTTCTGCCATCCTCTACCAC
Neogenin	TGACATGGCGTACACCTGCATC	GGCTGGTATTCTCAACACGCTC
DCC	CCACCTTCCAACTGGTACACAG	GAGAGGAGGTGTCCAACTCATG